Journal of Hydrology 664 (2026) 134461

Contents lists available at ScienceDirect

Journal of Hydrology

journal homepage: www.elsevier.com/locate/jhydrol

Hydrology of a cultivated peatland in Northern Finland and implications for management

Tung Pham [a,*], Hannu Marttila [a], Miika Läpikivi [a,b], Timo Lötjönen [b], Hermanni Aaltonen [c], Henriikka Vekuri [c], Bjørn Kløve [a], Maarit Liimatainen [a,b]

[a] Water, Energy and Environmental Engineering Research Unit, P.O. Box 8000, FI-90014, University of Oulu, Finland
[b] Natural Resources Institute Finland, Paavo Havaksentie 3, FI-90570 Oulu, Finland
[c] Finnish Meteorological Institute, Climate System Research Unit, P.O. Box 503, 00101 Helsinki, Finland

ARTICLE INFO

This manuscript was handled by Renato Morbidelli, Editor-in-Chief, with the assistance of Frédéric Huneau, Associate Editor

Keywords:
Organic soils
Groundwater table
Peat thickness
Controlled drainage
Agriculture
Northern regions
Water management

ABSTRACT

Peatlands are globally significant carbon storage and locally important for agriculture in Northern regions. However, cultivation on organic soils often results in nutrient leaching and greenhouse gas emissions. These impacts are strongly influenced by hydrology, yet the hydrological behavior of shallow peat soils (<1 m), which are common in many drained agricultural fields, remains understudied. In response, we studied hydrological processes in 6 fields with varying peat thickness (20–80 cm) over a mineral subsoil at the Ruukki NorPeat site in Northern Finland. The site features a controlled drainage system consisting of equally spaced perforated pipes installed at a depth of 120–130 cm within the mineral layer. Key hydrological variables, including groundwater table, soil moisture, drainage discharge, precipitation, evapotranspiration, and soil temperature, were continuously monitored from 2016 to 2021. Our results indicate that hydrological behavior strongly depends on seasonal climatic patterns, drainage management, and soil characteristics, particularly peat thickness. Plots with 60–80 cm peat thickness exhibited more stable groundwater tables and slower water table drawdown during dry periods, while thin peat plots (<30 cm) responded much more dramatically to hydrological inputs and losses, resembling behaviors of mineral soil. Despite prolonged drainage, the upper 30 cm peat layers remained a good buffer against short-term climatic variability and hydrological extremes. However, limited water storage in thinner peat makes these areas more susceptible to drought stress. Targeted measures such as earlier drainage closure or supplemental irrigation can be beneficial in these plots, though water table levels need to be balanced to maintain field trafficability.

1. Introduction

Peatlands, covering only about 4–4.9 million km^2, or 3 % of the Earth's land surface, play an important role in the global carbon cycle as significant natural carbon reservoirs (Xu et al., 2018). These ecosystems, classified as organic Histosols, are crucial for storing a substantial portion of the world's soil carbon (Drösler et al., 2008; Joint Research Centre: Institute for Environment and Sustainability, 2008). Beyond carbon sequestration, peatlands offer vital ecological services, including biodiversity preservation and water regulation, thus playing a pivotal role in ecosystem sustainability and climate change mitigation (Bonn et al., 2016), and are also important resources for food and biomass production.

In agriculture, organic soils form an important local resource. Peat soil has good inherent fertility and moisture retention capacity, thus drained peatlands can be highly productive. In Finland, approximately 300,000 ha, or 13.6 % of the total agricultural land, consist of organic soil, with up to 85,000 ha classified as peat soil (organic matter content ≥40 %) (Myllys and Sinkkonen 2004). In Northern Finland, organic soils can comprise up to 30 % of agricultural land (Virtanen, 2003). These statistics underscore the historical and ongoing regional importance of peatlands for food production and the national economy. However, the conversion of peatlands for agricultural use also creates notable environmental challenges. Pristine peatlands are water-saturated, thus drainage is required to lower the water table to a level suitable for cultivation. Nevertheless, drainage, along with other agricultural practices on peatlands, such as tillage and fertilization, are associated with increased greenhouse gas (GHG) emissions and nutrient leaching to

* Corresponding author.
E-mail address: thanh.pham@oulu.fi (T. Pham).

https://doi.org/10.1016/j.jhydrol.2025.134461
Received 12 May 2025; Received in revised form 30 September 2025; Accepted 20 October 2025
Available online 24 October 2025

nearby water bodies (Gerin et al., 2023; Pham et al., 2023). In cultivated peatlands, GHG and leaching dynamics are mainly driven by the hydrological characteristics of the site. Mechanistically, the groundwater table level (GWTL) governs the soil volumetric water content and thus biogeochemical processes, as deeper GWTL can lower soil moisture, increases O_2 diffusion and redox potential, and favors aerobic decomposition and nitrification, leading to increased CO_2 and N_2O production. Higher GWTL increases soil moisture, suppresses aerobic mineralization and N_2O, but enhances anoxic pathways and CH_4 production (Evans et al., 2021; Koch et al., 2023). Likewise, GWTL influences water quality, e.g., lower GWTL is connected with an increase in nitrate (NO_3^-) export via drains (Pham et al., 2023). By contrast, high or rising GWTL mobilizes dissolved organic carbon (DOC) to receiving streams (Rosset et al., 2022; Prijac et al., 2023). Beyond GWTL, soil structural features, such as layering, hydraulic conductivity anisotropy and macropore networks, control subsurface flow paths and residence times, which in turn modulate leaching of N and P (Rezanezhad et al., 2016; Gharedaghloo et al., 2018; McCarter et al., 2020; Wang et al., 2020).

Given their agricultural value and contribution to the farm-scale economy, raising the water table or rewetting these peatlands is not a straightforward decision. This reality necessitates a more comprehensive understanding of peatland hydrology and water management, to develop strategies that maintain agricultural productivity while minimizing environmental impacts. The balance between water retention and drainage, soil moisture content, and the depth of the groundwater table become crucial in managing GHG emissions and nutrient leaching. Yet, there is a notable gap in the thorough understanding of hydrological processes in cultivated peatlands, which hinders the ability to plan and implement effective water management measures (Maljanen et al., 2010; Maljanen et al., 2013; Regina et al., 2015; McCarter et al., 2020; Pham et al., 2023).

In response to this challenge, the Natural Resources Institute Finland (Luke) established the NorPeat research platform, located in Ruukki, Siikajoki, Finland, to study the hydrology of drained agricultural peatlands. The site features varying peat thickness and a controlled subsurface drainage system, making it ideal for continuous hydrological monitoring. Recent work at the NorPeat field has highlighted the important links between hydrologic state and other processes, including nutrient leaching through subsurface drains (Pham et al., 2023) and CO_2–N_2O emissions (Gerin et al., 2023). Modelling work for the site further shows that hydrological and biogeochemical responses depend on subsoil connectivity and peat thickness (Salla et al., 2024; Kajasilta et al., 2025). Thus, to address the knowledge gap and build on previous work of the site, our main objectives are: 1) to investigate the dynamics of the hydrological parameters in response to seasonal variations, soil structure, and controlled drainage practices; and 2) to establish a comprehensive water balance by quantifying water fluxes (evapotranspiration, drain flow, overland flow) to the adjacent stream.

2. Materials and methods

2.1. Site description

The NorPeat research facility (coordinates 64.684°N, 25.11°E) is located in the Siikajoki municipality, approximately 60 km southwest of Oulu, Finland. A detailed map of the study site, including the location and monitoring setup, is presented in Fig. 1. The platform spans an area of 26 ha, divided into 8 plots, varying in size from 2.79 to 3.77 ha. The scope of this study is on plots 1–6, as monitoring of the plots 7 & 8 was established later. The topography is characterized by a gentle slope of less than 0.5 %, and the elevation is about 45 m above sea level. Historical documents, including a 1933 soil map, confirm the area's continuous agricultural use for nearly a century. The research facility is affiliated with the European network for Analysis and Experimentation on Ecosystems (AnaEE 2025) and is actively managed by Luke.

The surface layer of the field is predominantly sedge peat, mixed with mineral soil. The thickness of the peat layer varies: in plots 1, 2, and 4, it ranges from 40 to 80 cm, while in plots 5 and 6, it averages approximately from 20 to less than 30 cm. Thus, the organic horizon of plots 5 and 6 does not meet the Finnish classification for peat soil (minimum of 30 cm thickness with at least 40 % organic matter content). Though, in this study, these plots will be referred to as thin peat plots. Plot 3 exhibits a combination of shallow peat and deeper layers up to 50 cm peat thickness. Below this, the subsoil consists of fine sand, silt, and silty clay. Sulfidic material is present in the subsoil beyond a depth of 1.0 m. Under the World Reference Base for Soil Resources (WRB), plots 1, 2, 4, and part of plot 3 are classified as Sapric Histosols (Sulfidic), and plots 5, 6, and part of plot 3 as Gleyic Histic Umbrisols (Sulfidic

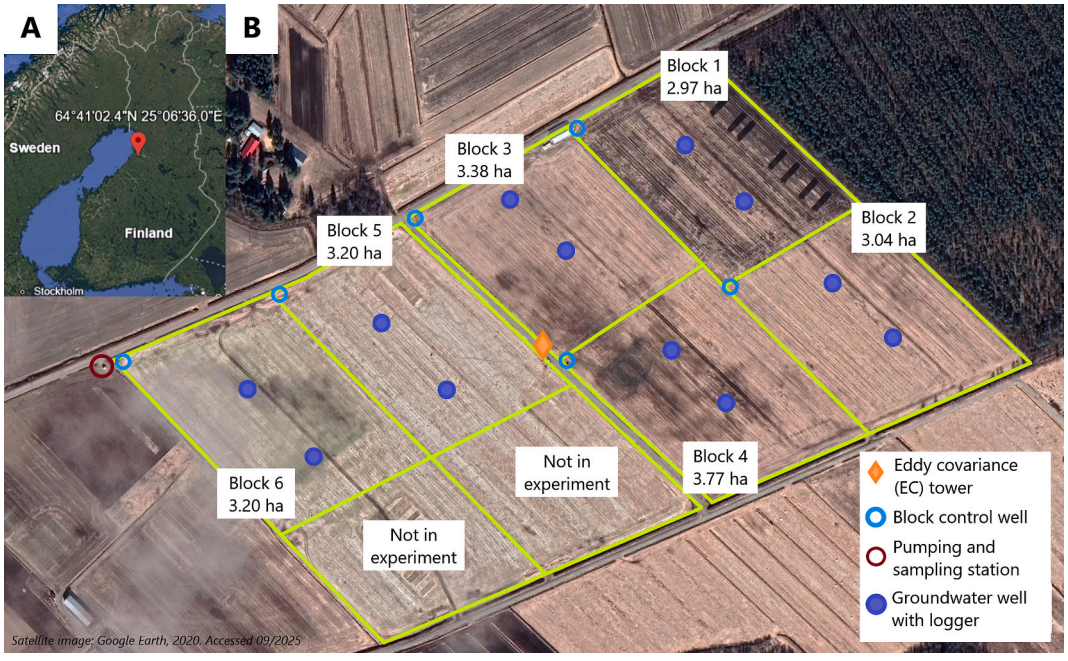

Fig. 1. Map and experimental setup of the Ruukki NorPeat field: A) location of the site; B) experimental setup and monitoring.

Thionic) (Yli-Halla et al., 2022). For hydrological comparison based on peat thickness, the field plots were divided into three groups: thick peat (60–80 cm), medium peat (30–60 cm), and thin peat (<30 cm).

The field features a drainage system of parallel lateral subsurface plastic pipes that channel water into collector drains, which then discharge into control wells (one per plot). The groundwater table (GWT) in each plot can be controlled by adjusting the outlet pipe height in control wells. This system prevents excessively low levels of GWT in the summer when the precipitation amount is much lower than evapotranspiration (ET). During the period of 2019–2021, the control system was in effect, and the wells were closed in all plots from early summer to mid- or late autumn (20 May–30 September in 2019; end of February–10 November in 2020, and 9 June–24 September in 2021).

Climatic data, including temperature and precipitation, is continuously monitored at a Finnish Meteorological Institute (FMI) weather station next to the field. According to the 30-year average (1991–2020), the average annual temperature at the site was 3.2 °C, with February typically being the coldest month (average −8.2 °C) and July the warmest (average 16.2 °C). The meteorological parameters of the field during the study period are presented in Fig. 2. Over this period, the annual average air temperature of the field area was 3.8 °C, slightly warmer than the long-term average. The temperature profile exhibits a clear seasonal pattern, with warmer summer months averaging 15 °C and cold winter periods averaging −6°C. During typical cold winters, snow cover begins to accumulate in early December, gradually increasing in depth through the season. The frozen ground period closely follows this timeline, lasting until snowmelt, which typically occurs between late March and early April as temperatures rise above freezing. Snow cover usually persists for 130 to 150 days, followed by a rapid decline in depth during melt. The growing season, with daily mean temperatures above 5 °C, usually lasts from early May to early October. During the winter of 2019–2020, abnormally warmer conditions (frequent fluctuations around 0 °C) led to multiple freeze–thaw cycles and intermittent snow cover. As for precipitation, during our study, the average annual precipitation was 562 mm, close to the 30-year average of 555 mm. The period of 2017–2019 was relatively drier (455–458 mm) and 2019–2021 experienced higher precipitation (669–684 mm). Precipitation is often low in early summer, with peaks in late July to August, and consistent lower amounts spread out from late autumn to spring.

The field has been primarily used for silage grass and cereal cultivation since 2016. Cultivated crops include perennial grass (timothy, meadow fescue) and cereal (barley). At times, the field was ploughed in the autumn and left bare during the winter. In 2020, all plots were uniformly growing silage grass, with two-stage mineral fertilization. The site employs conventional farm machinery for all farming activities. Detailed management of the field during the period of 2016 to 2021 has been previously reported by Yli-Halla et al. (2022) and Pham et al. (2023).

2.2. Hydrological measurements

The experimental plots originally employed open ditches for drainage, later transitioning to various subsurface drainage systems including wooden box drains (1900), clay pipes (1960), and plastic pipes (1980s onwards). The drainage system was gradually renewed over time between 1980 and 2016, with the latest renewal using plastic pipes installed in plots 1 and 2 due to non-functioning old drainage. These pipes were installed at a depth of 1.1–1.3 m, with a 12-meter spacing. Drainage laterals are connected to collectors that lead to a control well in each plot, from where water is directed to the sampling station at the corner of plot 6. Special attention was given to preventing clogging caused by rust precipitating in the drainage pipes, which can be flushed with equipped joint tubes accessible from the soil surface.

Monitoring of GWT utilizes perforated groundwater pipes (diameter Ø 50 mm), installed at a depth of 2 m in each field with Solinst Levelogger sensors in two pipes per plot. Barometric compensation was done using Solinst Barologger sensor's data, which is located inside the sampling station. The sensors captured GWT and atmospheric pressure at 15-minute intervals. These data are averaged to represent the GWT level for each plot. Additionally, twice per year, manual monitoring of GWT levels was conducted to complement continuous measurements.

Monitoring of soil moisture was conducted using Soil Scout moisture sensors (Hydra100 Scout, Soil Scout, Finland), installed at three depths (10, 30, and 50 cm) in each plot. The sensors recorded moisture readings at 20-minute intervals, with data automatically stored in a cloud database, enabling real-time online access. However, during the monitoring period, most of the sensors at 50 cm depth were either not yet in use or malfunctioning, resulting in limited data availability at this depth. Consequently, the data from 50 cm depth was excluded from the analysis.

Field discharge, including both subsurface (all plots) and overland flow (plot 6 only), is measured at the sampling station. A V-dam and water pressure sensor (STS PTM/N) are used to quantify the discharge volume, which is recorded as liters per hectare per day and stored

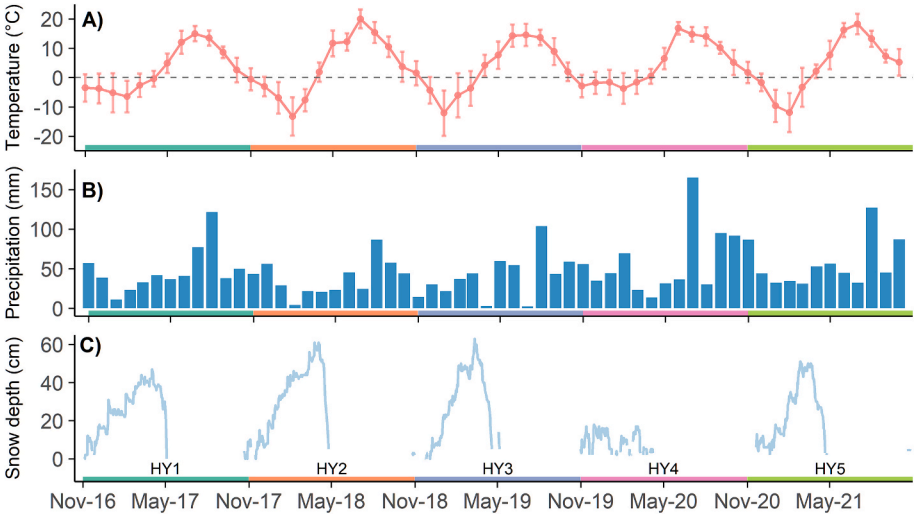

Fig. 2. Meteorological conditions at the field site during the 5-year monitoring period: A) average monthly air temperature (°C) with standard deviation (error bars), and a dashed horizontal line indicating the 0 °C threshold; B) total monthly precipitation (mm) and C) daily snow depth (cm). Hydrological years (November 1st–October 31st) are indicated by the shaded bars along the x-axis and labeled as HY1–HY5.

online. A customized system to pump the discharge water away from the sampling station was developed due to frequent higher water levels outside the station. This system consists of an electrical discharge pump (2.5 kW) with a design flow capacity of 20 l s^{-1} for the whole experimental field. In cases of extremely high flow, a tractor-driven hydraulic pump is used for flood control. Additionally, an automated system using pressurized air (3–4 bar) was established to clean the V-dam opening every 6 h to prevent interference of rust precipitation on the discharge measurement.

Soil hydrophysical characteristics, including bulk density (BD), soil water retention curve (pF) and horizontal saturated hydraulic conductivity (K_{sat}) were measured in all plots. Soil samples for BD analysis were collected with 55 cm^3 soil cores for every 10-cm depth up to 130 cm in all plots. BD samples were measured after drying at a constant temperature of 65 °C until no further significant weight changes were observed. For pF and K_{sat} measurements, a total of 21 peat samples were collected from various depths across all plots (25, 35, 70, and 75 cm depth in plots 1 to 4; 20 and 30 cm in plots 5; 10, 20, 30, and 40 cm in plot 6, due to the shallower peat thickness in plots 5 and 6). The K_{sat} was measured using flow cells while pressure chamber tests were used for pF with a similar method described in Menberu et al. (2021). All determinations for soil hydrophysical characteristics were conducted in the University of Oulu laboratories. Measured pF data (pressure head h and corresponding moisture content θ) was used to fit the van Genuchten soil water retention model (Eq. (1)) (van Genuchten, 1980). The model was calibrated for each sample using non-linear least squares optimization to minimize the sum of squared errors between observed and predicted water contents. The optimized parameters included the residual water content (θ_r), saturated water content (θ_s), inverse air-entry suction (α, in cm^{-1}), and the pore size distribution index (n). Within the optimization algorithm, θ_r was allowed to vary from 0 to 1.1 times the minimum measured water contents, θ_s was allowed to vary within the measured moisture content at saturation ± 10 %, α from 0 to 1 cm^{-1}, and n from 1 to 5. From the fitted model, volumetric water contents at field capacity (−10 kPa, or −102 cm H_2O for organic soil, and –33 kPa, or −336.5 cm H_2O for mineral soil) and permanent wilting point (−1500 kPa, or −15295.5 cm H_2O) were estimated. R^2 was calculated to assess model performance. Additionally, capillary rise was roughly approximated as the inverse of α to provide insight into pore-size-related water movement potential, based on the inverse relationship between pore radius and matric suction as described by the Young-Laplace equation (Jury and Horton, 2004).

$$\theta(h) = \theta_r + \frac{\theta_s - \theta_r}{[1 + (\alpha|h|)^n]^m} \; or \; \theta(h) = \theta_r + \frac{\theta_s - \theta_r}{[1 + (\alpha|h|)^n]^{1-\frac{1}{n}}} \quad (1)$$

In this study, ET data is used for the estimation of the water balance and the construction of the recession curve. The eddy covariance (EC) method is used to measure the turbulent fluxes of water vapor. The EC tower, located in the middle of the study site (Fig. 1), is operated by FMI. Its system consists of a 3D sonic anemometer (uSonic-3 Scientific, METEK Meteorologische Messtechnik GmbH, Germany) and an enclosed infrared gas analyzer (LI-7200, LI-COR Biosciences, NE, USA). The measurement setup is described in more detail in Gerin et al. (2023). Standard EC post-processing was applied, including de-spiking, block-averaging, double coordinate rotation and lag determination based on cross-correlation analysis (Rebmann et al., 2012). The systematic flux loss due to high-frequency attenuation was corrected for using the empirical method described by Laurila et al. (2005). Due to the differences in wind direction, the measured data was mostly available for the Southern side of the field (i.e., plots 5 and 6), while in the Northern side (plots 1–4) the data was scarcer. The data was screened according to the following quality criteria: number of spikes in the raw data <150, relative stationarity of the H_2O flux <50 % and variance of the H2O mixing ratio <0.5 (mmol mol^{-1})^2. In addition, measurements that did not sufficiently represent the target area were discarded by using the footprint model developed by Kormann and Meixner (2001) and setting the cumulative footprint limit to 0.7. Periods of weak turbulence were filtered using a friction velocity threshold estimated for CO_2 flux data (Gerin et al., 2023). We evaluated surface energy balance closure on the screened data and fitted a no-intercept regression of H + LE on R_n–G, where H = sensible heat flux, LE = latent heat flux, R_n = net radiation and G = ground heat flux. Here, we only used daytime conditions (R_n > 50 W m^{-2}). The fit yielded a slope α = 0.87, which is in the typical range (Mauder et al., 2024) and the residuals showed no clear dependence on relative humidity or air temperature. No post-hoc energy balance closure correction was applied, and the reported evapotranspiration sums are based on the unadjusted LE.

The data was gap-filled using a decision tree-based machine learning algorithm called extreme gradient boosting (Chen and Guestrin, 2016). We used an ensemble of 10 models and the hyperparameters of each model were optimized using 5-fold cross validation and randomized search. The environmental drivers included air temperature, photosynthetically active radiation, relative humidity, soil temperature at 5 cm depth and soil moisture at 10 cm depth. In addition, temporal drivers describing the seasonal and daily cycles were utilized (Vekuri et al., 2023).

The water balance for the site can be written as:

$$P = D_{out} + ET_a + (O_{out} + D_p + \Delta S) \quad (2)$$

in which P is the direct precipitation amount upon the site area, D_{out} is the amount of water discharged through the subsurface drainage system, O_{out} is the amount of overland outflow, ET_a is the actual evapotranspiration amount, D_p is the amount of infiltrated water below the drainage pipes (which can then contribute to groundwater recharge or move laterally through subsoil layers) and ΔS is a change in water storage within the soil profile. Since only P, D_{out}, ET_a and soil moisture within the upper 30 cm were directly measured, and O_{out} was measured only in plot 6, O_{out}, D_p and ΔS were not explicitly quantified for all plots. Instead, their combined effect was estimated as a whole, representing the unmeasured portion of the water balance in our study.

Between rainfall events, GWT declines due to water output (e.g., from drainage and ET) exceeding input, which is defined as a recession period. In practice, recession events are periodically interrupted by subsequent rainfall events which raise the GWT, thus a master recession curve (MRC) can be constructed by aligning multiple recession events, to illustrate how GWT can recede throughout the soil profile if there is no interruption from rainfall. Similarly, the concept can be applied to the recession periods of subsurface discharge, forming a master recession which shows how the discharge rates decline from their highest level. In this study, the MRC for GWT and discharge is constructed using the matching strip method, adapted from Cobb et al. (2017) and Cobb and Harvey (2019). The start of the MRC (day 0) is set to be at the shallowest recorded GWT, or the highest level of subsurface discharge rate.

The hydrological year at the site was defined from November 1st to October 31st, with the monitoring period spanning five full hydrological years, from November 1st, 2016 (Hydrological Year 1) to October 31st, 2021 (Hydrological Year 5). This timeframe ensures that the hydrological year starts after the primary growing season, when evapotranspiration rate declines, and precipitation has been accumulated in soil. Additionally, defining the year starting from November 1st ensures that the entire snow season, from the onset of snow accumulation though spring melt, is fully captured within a given hydrological year.

3. Results

3.1. Soil hydrophysical characteristics

The results of soil physical characteristics are presented in Table 1 and Table S1. In our study site, BD measurements vary notably across soil types, from 0.2 to 0.7 g cm^{-3} (organic soil) and ~1.6 g cm^{-3} (upper

mineral soil region). In plots 1–4, the peat layer retains sufficient thickness, that differences between the surface and lower peat layer could be observed. In thin peat plot (5, 6), the entire organic layer (~30 cm) exhibits similar characteristics comparable to the upper peat layer of plots 1–4, except for notably lower SOM content (<40 %). This soil can also be observed to often contain traces of sand. In general, compared to the lower peat layer, the upper layer has significantly less SOM content, higher BD, slightly less porous, lower horizontal K_{sat} and able to retain less moisture. In all plots, the mineral layer beneath the organic topsoil is sandy soil, with minimal variability in characteristics between the plots in SOM, BD and porosity. In this layer, there are numerous visible traces of empty old root channels, which have important implications for water infiltration, as estimated horizontal K_{sat} are low across the field and depths, ranging from 8.7×10^{-8} to 6.7×10^{-7} m s^{-1}.

The soil water retention capacity results are presented in Table 1, Table S1 and Fig. S1. Good moisture retention can be observed throughout the profile, with surface peat holding approximately 60 % at field capacity, and ~77 % in lower peat layers. This good retention capacity extends to permanent wilting point as well (~29–44 % for the upper peat and ~32–52 % for the lower peat layer). The water retention profile of organic soil is consistent across plots. Drainable porosity is estimated at 5–23 %, and plant available water content at 17–37 % in the peat layer. For the mineral layer, in plots with thicker peat layers (e.g., plots 1 and 2), the underlying mineral soil also shows slightly better water retention near field capacity (~25–30 %) compared to the remainder of the plots (10–15 %), despite similar values in all other parameters (Table S1).

3.2. Groundwater table level dynamics

In our study site, the behavior of the groundwater table level (GWTL) is distinctive between plots with different peat thicknesses. The annual and overall summary statistics for GWTL across different peat thickness categories are presented in Table 2. Across all years during 2018–2021, peat thickness was strongly associated with GWTL. Thick peat consistently maintained the shallowest GWTLs (overall mean: −76 cm), followed by medium (−83 cm) and thin peat (−96 cm). This pattern was held in each year, although absolute depths varied as climate factors changed (most notably precipitation and ET). This ranking also applies to GWTL variability, as thin peat plots had some of the deepest (as low as −200 cm or more, beyond logger range) and shallowest GWTLs (~2 cm, water pooling events), while thick peat remained the most stable.

The GWTL also showed clear seasonal dynamics across all peat thickness groups (Fig. 3A). During the typical snow season (December–March), all three peat thicknesses maintained shallower water tables with free drainage (above the drainage pipes). Snowmelt during April–May sharply increased the GWTL due to high water input, though the response was more gradual in thick peat. Free drainage effectively lowered the water table back to pre-melt levels by June, making the soil suitable for cultivation. From late May through August, increasing ET and low rainfall caused GWTL to reach their annual minimum. Autumn rainfall (beginning in late July) and closed drainage recovered the GWTL, especially where earlier drawdown was most severe. By early winter, water tables stabilized again around −70 to −80 cm across the field. Throughout the year, the relative pattern between peat thickness classes remained consistent with thick peat maintaining the shallowest and most stable GWTL, followed by medium and thin peat.

Fig. 4A shows the temporal distribution of GWTL across the study period. In thick peat areas, GWTL dynamics were highly stable, as indicated by the gradual slope and smooth S-shaped form of the curve. As peat thickness decreased, this S-shape became less defined, with steeper slopes indicating more rapid fluctuations and reduced stability. Across all plots, GWTL rarely remained near the soil surface for extended periods, as shown by the rapid recession from peak levels following high water tables, as seen in Figs. 3A, Fig. 4A, and Fig. 5. These dynamics

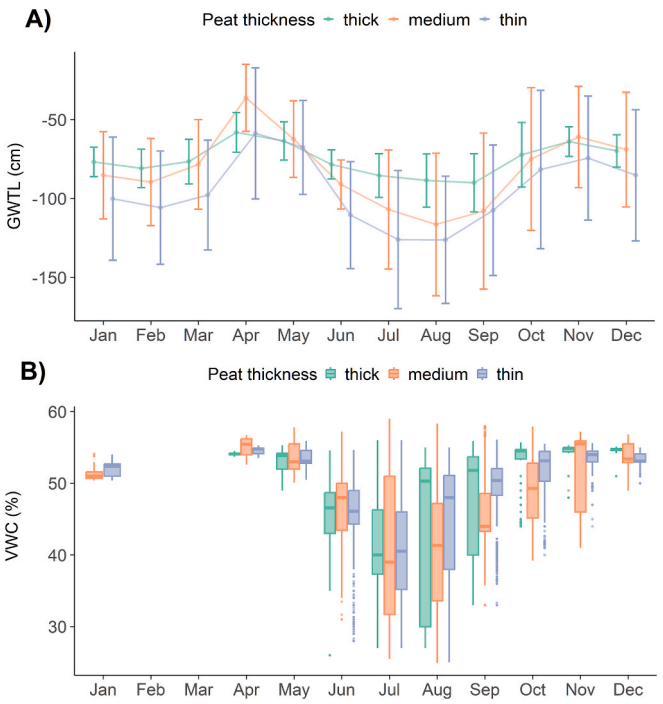

Fig. 3. A) Multi-year monthly average groundwater table depth (cm) across peat thickness groups, with error bars indicating ± 1 standard deviation from the mean, and B) box plots of soil moisture (%) in the top 30 cm of the soil profile, shown by month and peat thickness group. Each box represents the median, interquartile range, and whiskers extending to 1.5 times the interquartile range; outliers are shown as individual points.

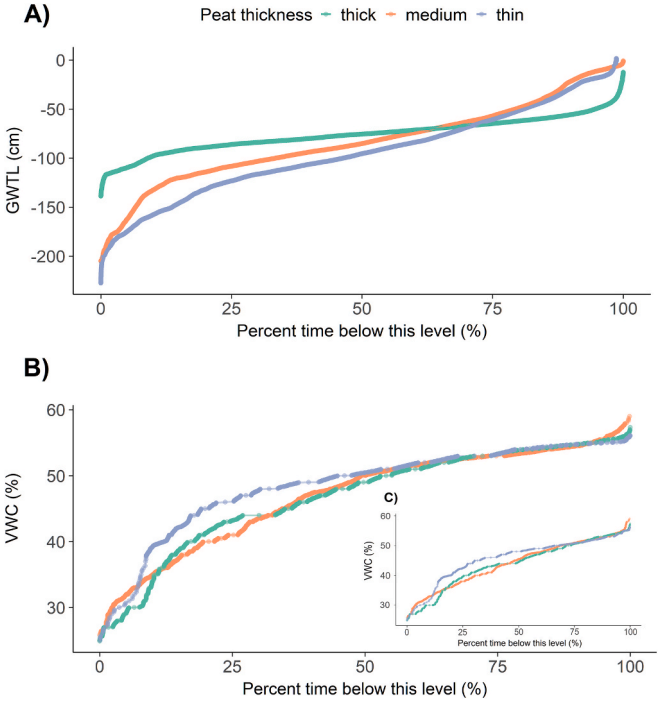

Fig. 4. A) Time residence curve of groundwater level across 3 peat depth categories. B) Time residence curve of the top 30 cm soil moisture, across 3 peat depth categories. C) Time residence curve of the top 30 cm soil moisture, across 3 peat depth categories during the warmer season with elevated evapotranspiration level (June–September).

suggest that topsoil saturation was generally short-lived. Notably, the inflection points and changes in curve slope visible in Fig. 4A correspond to transitions in peat physical properties with depth, particularly porosity and water retention capacity (Table 1).

In the MRC (Fig. 5), which isolates the drainage-driven decline in GWTL by removing the effects of rainfall, behavior of GWTL drawdown influenced by peat thickness can be observed. In general, GWTL is drawn down quickly within the peat zones, particularly the upper peat layer. In thick peat plots, recession rates were both slower and more consistent, with similar slopes observed under both free drainage (WO) and restricted drainage (WC) conditions. In these plots, the upper peat layer (up to ~50 cm depth) exhibited the highest recession rates, which is higher than the mineral subsoil beneath. Below ~60–70 cm depth (lower peat and mineral subsoil zones), recession rates declined and remained stable. In thinner and medium peat plots, GWTL recession occurred much more rapidly. However, the pattern of similar recession behavior between open and closed drainage persisted. The steepest declines were typically observed in the peat and sandy subsoil layers, while the deeper silty or clayey subsoil layers showed a moderate slowing of recession (Table 3).

3.3. Soil moisture dynamics

Monthly average soil moisture for the top 30 cm across three peat thickness categories is presented in Fig. 3B. Moisture in the topsoil exhibits seasonal variation comparable to GWTL. From the second half of December to the end of March, accurate soil moisture measurement was generally not possible, due to topsoil freezing, leading to the sensors not working correctly. An exception to this occurred during the mild winter of 2019–2020, during which some moisture measurements could be obtained during freeze–thaw periods in December and January. Between April and July, increased ET led to marked declines in moisture content, most notably in thin peat areas. During this period, medium and thick peat areas maintained comparatively higher and more stable moisture levels despite similar drying conditions. During August–September, soil moisture variability increased across all peat thickness categories, as autumn precipitation replenished moisture content. In October–November, with reduced ET, moisture levels gradually rose and stabilized. Thick peat consistently displayed the lowest variability throughout, while medium and thin peat showed greater fluctuations, especially during the summer months.

Soil moisture time distribution curves (Fig. 4B) show consistent water retention capacity in the top organic layer across all peat thicknesses. Moisture remained above 50 % (approximately field capacity) roughly half the time and only dropped below 40 % (near permanent wilting point) for 10–17 % of the total observations. Although minor differences between peat thickness categories occurred in drier periods, with thin peat slightly wetter than medium or thick peat, these differences were subtle and do not strongly suggest moisture stability is directly related to peat thickness. This result is coherent with the similarity in top peat physical characteristics in Table 1.

3.4. Runoff (subsurface discharge and overland flow) dynamics

Subsurface discharge patterns observed at our study site are shown in Fig. 6. Discharge exhibited distinct seasonal dynamics, characterized by rapid responses during the snowmelt period (April-May), resulting in steep hydrograph slopes and high peak flows. Approximately 38 % of annual subsurface discharge occurred within these few weeks. During summer, when drainage wells were typically closed, subsurface discharge was minimal or absent except during occasional intense storms (e.g., August 2020; Fig. 2). Once the wells were reopened, subsurface discharge resumed to lower rates through autumn and even continued at low levels during winter despite frozen ground conditions. Frequent freeze–thaw cycles during winter 2019–2020 disrupted typical single snowmelt peaks, instead resulting in multiple smaller discharge events throughout winter.

Although monthly discharge patterns were broadly consistent across the site, peat thickness significantly influenced discharge magnitude and variability (Figs. 6 and 7). Thick peat areas generally produced higher discharge rates, greater variability, and more pronounced peak flows. Subsurface flow persisted throughout winter months across all peat thicknesses, especially during warmer winters with increased snowmelt (winter 2019–2020).

Overland flow consistently remained lower than subsurface discharge across all months, mostly occurring during snowmelt or high-intensity rainfall events, with a maximum recorded rate of approximately 13 mm. The annual average overland flow was 54 mm, representing roughly 9.6 % of input precipitation. This highlights that subsurface drainage dominates runoff processes at the site.

Peat thickness also affected the recession behavior of subsurface discharge (Fig. 7). In thick peat plots (plots 1 and 2), discharge rates were higher and receded slowly after peak events. In contrast, thin peat plots (plots 5 and 6) had rapid recession, with discharge quickly dropping to near-zero within approximately one week. There are also some notable differences in recession behaviors among plots within the same peat thickness category. For example, plot 2 exhibited somewhat faster recession than plot 1, though this is possibly due to localized areas of thinner peat within plot 2. Similarly, plot 5 displayed a more gradual and stable recession pattern compared to plot 6, despite both plots having fairly similar soil structure.

3.5. Water balance

As ET data is only available during the last two years of monitoring, water balance could only be properly established during this period. During these years, the whole field ET and subsurface discharge amount remained similar. Due to a reduction in precipitation in the last year, the net storage change shifted from a slight positive in 2019–2020 to a slight deficit in 2020–2021. The water balance result supports the dominance of subsurface flow in this field as the dominant runoff process, and the significance of ET as water output during the growing season when the subsurface discharge is minimal. The generation of subsurface runoff is noticeably more efficient as peat thickness increases, evidenced by the higher proportion of water input as discharge in this water balance, as

Table 1
Summary of soil hydrophysical properties across all 6 plots at various depth ranges, including soil organic matter content (SOM), porosity, bulk density (BD), horizontal saturated hydraulic conductivity (K_{sat}), soil moisture retention at saturation (θ_s), field capacity (θ_{fc}), and permanent wilting point (θ_{pwp}). Layers' depth range are approximately ± 5 cm depending on the location in the field. The mineral layer starts at ~40–70 cm from the surface, depending on the peat thickness. Full detailed data along with SWRC fitted parameters are presented in Table S1.

Plot	Layer	SOM (%)	Porosity (%)	BD (g cm^{-3})	K_{sat} (m s^{-1})	θ_s (%)	θ_{fc} (%)	θ_{pwp} (%)
Thick peat (plot 1, 2)	Upper peat (0–30 cm)	43.5	81.9	0.5	1.3×10^{-7}	74.4	59.5	33.5
Thick peat (plot 1, 2)	Lower peat (30–70 cm)	83.7	93.3	0.2	8.7×10^{-8}	88.1	76.9	40.8
Medium peat (plot 3, 4)	Upper peat (0–30 cm)	41.2	78.6	0.6	6.7×10^{-7}	69.7	60.9	36.2
Medium peat (plot 3, 4)	Lower peat (30–50 cm)	82.4	91.9	0.2	2.1×10^{-7}	85.4	77.7	46.7
Thin peat (plot 5, 6)	Peat (0–30 cm)	34.2	74.7	0.7	3.4×10^{-7}	66.6	58.6	36.4
All plots	Upper mineral	0.7	38.5	1.6	8.9×10^{-8}	37.1	27.5	7.5

Table 2
Annual average water table depth (WTD) values (cm) across peat thickness categories (2018–2021). Thick peat is classified as having 60 cm or more of peat in topsoil, medium as 30–60 cm, and thin as less than 30 cm.

Year	Peat Thickness	Mean WTD (cm)	Median WTD (cm)	Min WTD (cm)	Max WTD (cm)
2018	thick	−78.0	−77.9	−119.6	−15.9
2018	medium	−107.6	−104.2	−195.9	−1.2
2018	thin	−124.7	−126.1	−202.0	−9.9
2019	thick	−85.0	−84.2	−138.9	−22.4
2019	medium	−104.9	−105.6	−205.1	−9.6
2019	thin	−106.2	−104.9	−205.5	0.0
2020	thick	−69.9	−68.8	−105.5	−12.4
2020	medium	−49.5	−52.0	−113.3	−0.7
2020	thin	−77.8	−75.5	−227.6	1.7
2021	thick	−72.6	−73.0	−115.0	−19.9
2021	medium	−73.1	−76.7	−158.7	−2.3
2021	thin	−82.8	−84.5	−194.7	−0.2
3-year	thick	−76.3	−75.6	−138.9	−12.4
3-year	medium	−83.4	−85.2	−205.1	−0.7
3-year	thin	−95.5	−96.3	−227.6	1.7

well as higher runoff ratios reported in the previous study (Pham et al., 2023).

4. Discussion

4.1. Impact of peat depth and soil characteristics on moisture and GWTL dynamics

During the monitoring period, we observed that the dynamics of the GWTL varied with peat thickness. Measurements showed that thicker peat layers maintained shallower and more stable GWTL with reduced annual variability. This suggests a strong buffering effect of the peat layer, in line with previous findings (Minkkinen and Laine, 1998; Berglund and Berglund, 2011). This buffering effect is largely driven by the physical properties of peat soils, as low BD and high porosity mean higher water storage capacity and stronger capillary force to retain moisture, particularly under limited precipitation periods. This is notable in thick and medium peat plots, where the lower peat zone has much lower BD and higher porosity than the upper zone, as measured water retention capacity is larger here. As thin peat plots only have the organic horizon with characteristics similar to other plots' upper peat, this explains why the GWTL in these plots were generally deeper with more variability. In addition, the upper mineral soil in thick peat plots also has better water retention capacity than in thin peat, which could supply moisture upward between rains via capillary action and help keep the GWTL shallow and stable.

In our field, the properties of the layered mineral subsoil could influence how easily water reaches the drains. As the drainage laterals are located in a silty layer at ~1.1–1.3 m depth, the hydraulic conductivity and thickness of this silt are the main constraint on both the magnitude and the rate of groundwater drawdown achieved by the drains (van der Molen and Wesseling, 1991; Ritzema, 2006). Where peat is thin and the underlying silt is thick, the hydraulic connection to the drains is more efficient, but storage is small, thus heads drop quickly after rain and recession limbs are shorter and steeper. The total subsurface discharge is smaller due to the limited drainable storage in thin peat (Rezanezhad et al., 2016; Menberu et al., 2021). In plots where the peat is thick but the silty layer at drain depth is thin with clay lying below, the pathway to the pipes can be more restrictive. This could contribute to the GWTL remaining more perched in the peat and receding more slowly. The larger drainable storage in thick peat and the longer drainage duration could also lead to greater cumulative subsurface discharge (Minkkinen and Laine, 1998; Berglund and Berglund, 2011; Morris et al., 2022). Because the clay layer dips more steeply than the ground surface, pressure slope could develop and direct water toward areas where the silt is thickest and the clay is deepest. This focuses fast, sharp responses in the thin peat over thick silt plots but does not change the observed pattern that total subsurface discharge increases with peat thickness (Ritzema, 2006).

Our laboratory measurements of K_{sat} showed slow horizontal water movement within all soil profiles. The low horizontal K_{sat} in peat has previously been reported, and the result of our study is comparable to prior measurements in Northern agricultural peatlands (Menberu et al., 2021; Morris et al., 2022). This coupled with the flatness of the field (slope <0.5 %) implies that there was a limited amount of lateral water movement within the peat matrix or the mineral subsoil region above the drainage pipe. Together, this evidence suggests there may have been a small effect of horizontal water transport on the overall water balance of the field. In addition, previous study of cultivated peatland with controlled drainage has also suggested a significant effect of horizontal water transport, which is important in periods of limited drainage (Tähtikarhu et al., 2025). As horizontal K_{sat} was only measured down to 75 cm, horizontal water movement may occur to a limited extent above this depth, although this may not necessarily apply to the region below it, extending down to the drainage depth. This effect, along with high ET loss and lower water storage capacity, may explain why the GWTL in thin peat plots continued receding down to −200 cm and below during periods of limited precipitation. Additionally, in a previous modelling study of the same site, it was strongly suggested there exists a significant additional water input from the adjacent peatland forest site to plot 1 (thick peat plot) (Salla et al., 2024). The effect of this potential additional water input could help to explain the large difference between the subsurface discharge amount between plot 1 and 2 (both are thick peat plots). However, this large difference in the subsurface discharge was only apparent in plot 1, suggesting low K_{sat} and small slope may contribute to limiting the effect of this water source mainly in plot 1.

On the other hand, the field generally exhibits good water vertical movement, as GWTL typically responded quickly to precipitation events, coupled with quick recession speed in all plots. Typically, natural peatland is anisotropic, with horizontal K_{sat} exceeding vertical K_{sat}, though in drained peatlands the difference might be minimal (Rezanezhad et al., 2016; McCarter et al., 2020). Though, even if the peat is isotropic due to extended drainage, it is clear that K_{sat} alone cannot fully explain the vertical movement of water in our field. This suggests the major role of macropores and empty root channels in vertical water transport. The prevalence of empty root channels extending to the subsoil deeper than 1 m has been reported in a previous study of the same field, and the significance of macropores and empty root channels in vertical water transport is well documented (Wallage and Holden, 2011; McCarter et al., 2020; Pham et al., 2023).

In our study site, as GWTL was mostly under 30 cm, which is also the limit of the peat depth in the thin peat plots (plot 5, 6), it justifies the differences in hydrological behavior between these plots and the remainder of the field. With our field's GWTL dynamics, hydrological

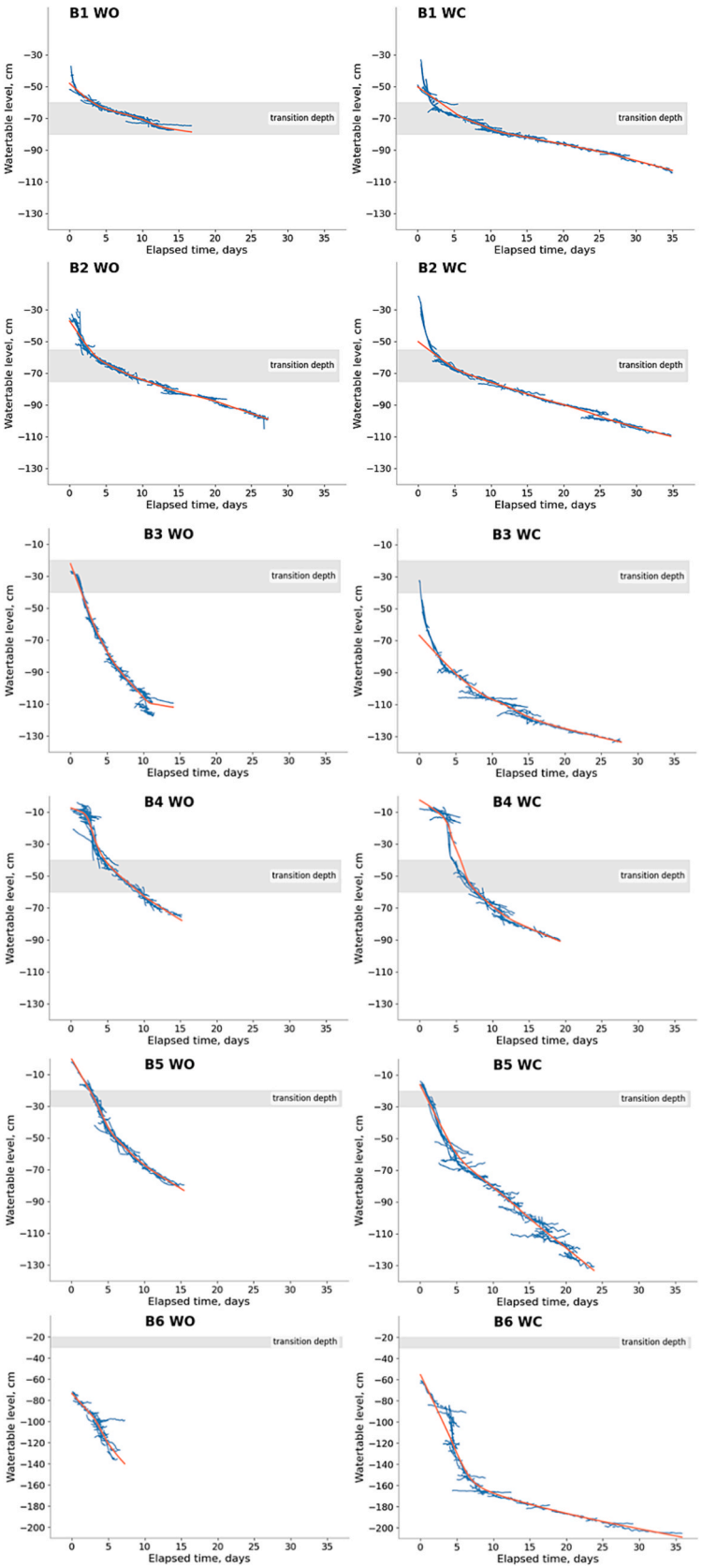

(caption on next page)

Fig. 5. Master recession curves constructed for each of the field plots (B1–B6 as for plot 1 to 6), i.e., how the ground water table level (GWTL) would decline throughout the soil profile without water input events. The master recession curves start at the point of highest GWTL observed for each plot (time Day 0). The recession is separated into duration during which the drainage wells were open for free drainage (WO) and closed during the summer to minimize drainage (WC). Shaded areas annotated "transition depth" depict the approximate depth range where the transition between the peat topsoil to the mineral subsoil could be found. Orange line depicts smoothing line using Loess regression. (For interpretation of the references to colour in this figure legend, the reader is referred to the web version of this article.)

Table 3
Water balance components in the last two hydrological year of monitoring, presenting annual totals for precipitation, evapotranspiration (ET), subsurface discharge, and the sum of overland flow + net storage change + deep percolation ($O_{out} + D_p + \Delta S$) (except for plot 6 where O_{out} was directly measured), also with a percentage of total precipitation for each year.

Block	Water balance component	2019–2020	2020 – 2021
	Precipitation (P)	661 mm (100 %)	598 mm (100 %)
1	ET_a	350 mm (53 %)	361 mm (60 %)
	D_{out}	506 mm (77 %)	450 mm (75 %)
	$O_{out} + D_p + \Delta S$	−195 mm (−30 %)	−213 mm (−35 %)
2	ET_a	350 mm (53 %)	361 mm (60 %)
	D_{out}	296 mm (45 %)	315 mm (53 %)
	$O_{out} + D_p + \Delta S$	15 mm (2 %)	−78 mm (−13 %)
3	ET_a	350 mm (53 %)	361 mm (60 %)
	D_{out}	256 mm (39 %)	221 mm (37 %)
	$O_{out} + D_p + \Delta S$	55 mm (8 %)	16 mm (3 %)
4	ET_a	350 mm (53 %)	361 mm (60 %)
	D_{out}	269 mm (41 %)	311 mm (52 %)
	$O_{out} + D_p + \Delta S$	42 mm (6 %)	−74 mm (−12 %)
5	ET_a	325 mm (49 %)	325 mm (54 %)
	D_{out}	151 mm (23 %)	211 mm (35 %)
	$O_{out} + D_p + \Delta S$	185 mm (28 %)	62 mm (11 %)
6	ET_a	325 mm (49 %)	325 mm (54 %)
	D_{out}	223 mm (34 %)	216 mm (36 %)
	O_{out}	75 mm (11 %)	23 mm (4 %)
	$D_p + \Delta S$	38 mm (6 %)	34 mm (6 %)
Whole field	ET_a	342 mm (52 %)	349 mm (58 %)
	D_{out}	280 mm (42 %)	285 mm (48 %)
	$O_{out} + D_p + \Delta S$	39 mm (6 %)	−36 mm (−6%)

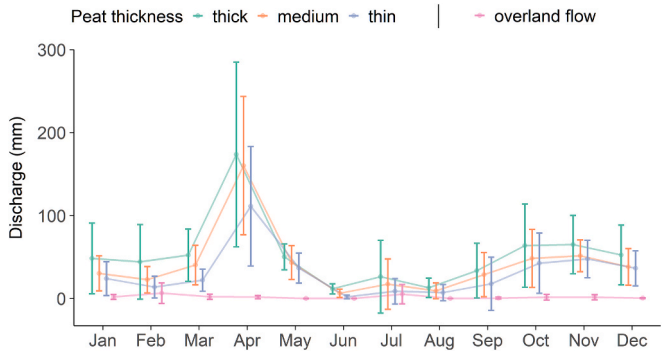

Fig. 6. Monthly average discharge (mm) for different peat thickness categories (thick, medium, thin) and surface runoff. Thick peat is classified as having 60 cm or more of peat topsoil, medium as 30–60 cm, and thin as less than 30 cm. The x-axis represents the months of the year, the y-axis shows the monthly average specific discharge values. Vertical error bars indicate the standard deviation for each category. Surface runoff, independent of peat thickness, is included as a distinct category to allow for comparison.

processes would mostly occur in the mineral soil, while in other plots there would be processes happening in both the peat and mineral layers. The differences would be the most obvious between the thick and the thin peat plots (plots 1, 2 vs. 5, 6), as in thick peat, the GWTL was largely varying within the peat zone. Therefore, comparing thin peat plots to thick peat plots at our site is essentially a comparison between mineral and peat–mineral systems.

In our study, soil moisture behavior in the top 30 cm was comparable across all plots, despite clear differences in GWTL between them. This suggests that the upper peat layer has a strong water retention capacity that buffers moisture levels from fluctuations in the deeper groundwater table. This is likely due to the similarity in peat characteristics within the top 30 cm, where the soil moisture sensors were installed. In contrast, the peat layer below this depth shows more variability in properties, and thus the moisture dynamics are expected to differ. Including moisture measurements from deeper layers in future studies would help clarify how peat thickness and subsoil characteristics influence soil moisture distribution patterns. This would be especially relevant for understanding subsurface hydrological and biogeochemical processes. Additional moisture data from deeper layers would also improve the estimation of water storage changes for water balance analysis and help isolate horizontal flow or deep percolation.

4.2. Water balance and runoff are controlled by climatic and drainage conditions

The patterns of subsurface discharge in our field respond to climatic inputs and connect to the physical properties of the soil, particularly peat thickness. During the last two hydrological years, when water balance could be established, precipitation was relatively abundant compared to the 30-year average. However, the distribution of water among the other components varied significantly across different blocks, corresponding to variations in peat thickness.

For subsurface discharge, thicker peat plots showed higher specific discharge rates compared to blocks with medium and thin peat. Understandably, this corresponds to the higher water storage capacity in these soils due to higher porosity, and the presence of macropores/root channel helping the rate of water transmission (Holden et al., 2006; Wallage and Holden, 2011; Rezanezhad et al., 2016). Macropores and root channels possibly explain why subsurface runoff in these plots was flashy (i.e., discharge rates responded quickly to water input events). The installation of the drainage system has altered the soil structure above the drainage pipes, resulting in a softer soil matrix partially filled with sand. This coarser, less compacted layer likely enhances infiltration and accelerates subsurface flow. Such rapid hydrological responses were especially evident during periods of high water input, such as snowmelt. The persistence of subsurface discharge during frozen winter months also suggests that water movement continues through unfrozen soil layers or via preferential flow paths despite surface freezing. During the mild winters or at the end of winter, the soil frost is often uneven and full of holes, so it is also possible that surface water flows to drainage pipes during these periods. These phenomena indicate that the generation of subsurface discharge is active year-round and only depends on the management of the drainage well.

In our field, overland flow was observed to be a minor proportion of runoff, and primarily occurring during snowmelt or intense rainfall events, as when the infiltration capacity of the soil is exceeded. The limited quantity of overland flow was typical of drained, flat peatlands, as the non-saturated peat layer promotes infiltration and subsurface flow and significantly reduces the generation of near-surface saturated overland flow (Holden et al., 2006).

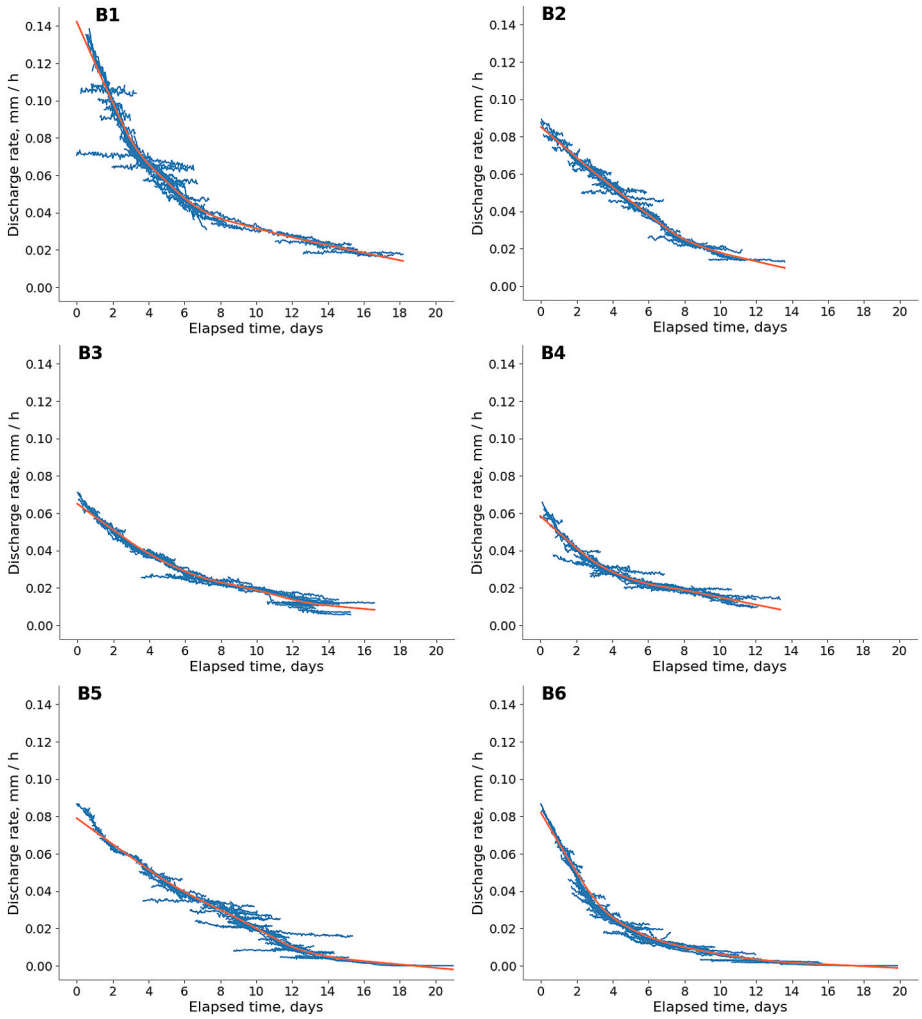

Fig. 7. Master recession curves of discharge rate in each of the field plots (B1–B6 as for plot 1 to 6), i.e., how the discharge rates (as mm h^{-1}, 1 mm h^{-1} = 10 m^3 h^{-1} ha^{-1}) would continuously decline with time and without interruption from water input events. The curves start at the point of highest discharge rate observed for each plot. Orange line depicts smoothing line using Loess regression. (For interpretation of the references to colour in this figure legend, the reader is referred to the web version of this article.)

4.3. Implications to soil biochemical processes and sustainable field management

Hydrology controls the availability of water, oxygen, and alternative electron acceptors in peat soils. Therefore, the findings of our study can have significant implications for the management of GWTL in cultivated peatlands. The observed differences in hydrological dynamics caused by peat thickness and soil physical properties imply the need for flexible water management practices depending on the soil conditions. In areas with thicker peat layers, current management practices have been sufficient in maintaining shallower water tables and good soil moisture availability. The high water retention capacity of thick peat layers buffers against hydrological fluctuations, supporting crop growth and reducing the risk of peat degradation. However, in areas with thinner peat layers, a more careful regulation of drainage systems or an addition of water via irrigation should be considered to prevent excessive lowering of the GWTL. Excessively low GWTL in thin peat areas can lead to peat oxidation and subsidence, increasing GHG emissions, particularly CO_2, due to increased aerobic decomposition of organic matter (Evans et al., 2021). Additionally, the presence of acid sulfate materials in the subsoil also becomes more prone to oxidation during periods of low GWTL, potentially leading to large amount of acidity in the drainage discharge (Yli-Halla et al., 2022, Pham et al., 2023).

The depth of the GWTL influences redox conditions and microbial activity within the soil profile. This impacts the cycling of nutrients such as N and P, as well as the generation of GHGs. A shallower GWTL creates more anoxic conditions, which suppress aerobic decomposition and nitrification, reducing CO_2 production and NO_3^- formation, while also mobilize P via Fe(III) reduction (Reddy et al., 2022). Anoxia promotes denitrification and, under prolonged saturation, methanogenesis, increasing N_2O and CH_4 emissions (Maljanen et al., 2010). Conversely, a deeper GWTL promotes aerobic conditions, enhancing peat decomposition, increasing CO_2 release and NO_3^- production, and contributing to subsidence, while generally reducing P mobility through sorption to Fe/Al oxides (Grønlund et al., 2008; Reddy et al., 2022). Therefore, managing the GWTL is a delicate balancing act, so that the GWTL stay at the proper level to prevent both prolonged anoxic conditions (risk of P release, N_2O/CH_4 emissions) and excessive aerobic conditions (enhanced nitrification and peat loss).

Fluctuating water tables can also lead to the mobilization of leachable N and P. Dry conditions promote the decomposition of organic matter and accumulation of mineralized nutrients. When the soil is rewetted, there can be a flush of NO_3^- and phosphate (PO_4^{3-}) as microbial activity resumes, increasing nutrient leaching, and potentially leading to groundwater contamination and eutrophication of downstream water bodies (Zak et al., 2010). Maintaining a stable GWTL reduces these fluctuations and increases nutrient retention in the soil.

Our study site represents a typical agricultural field with

heterogeneous peat thickness. As shown by the results, the variability in peat thickness can affect how different areas of the field would respond to uniform controlled drainage practices. Particular attention should be given to plots with thinner peat, where the capacity to buffer water loss during the growing season is much reduced. In addition, closing the drainage well during warmer periods was not sufficient to maintain a shallow groundwater table, potentially leading to unwanted oxidation of peat and acid sulfate materials in the subsoil. To mitigate this, additional measures such as earlier well closure or targeted irrigation in vulnerable plots may be beneficial. However, it is important to avoid excessive water levels, which can reduce the soil's load-bearing capacity and hinder field operations.

Lastly, anticipated increases in temperature and evapotranspiration under climate change scenarios may worsen soil moisture deficits in drained peatlands (IPCC, 2014). Proactive management strategies that enhance soil water retention, such as maintaining vegetation cover and reducing drainage intensity can improve resilience to climatic variability (Limpens et al., 2008). This approach aligns with broader efforts to adapt agricultural practices to the impacts of climate change, improving the long-term sustainability of peatland ecosystems.

5. Conclusions

The hydrology of cultivated peatlands is strongly influenced by climate, drainage management, and soil properties, most notably peat thickness. Our study demonstrated that peat thickness affects groundwater fluctuations, soil moisture dynamics, and runoff responses under controlled drainage. Thick peat plots (60–80 cm) maintained shallower, more stable groundwater tables and slower drawdown rates during dry periods. In contrast, thin peat plots (<30 cm) responded more quickly and variably to hydrological inputs and losses, resembling the behavior of mineral soils. The upper 30 cm of peat retained good moisture regardless of thickness, providing a short-term buffer against climatic extremes. However, limited water storage in thinner peat made these areas more vulnerable to drought stress, suggesting the need for adaptive, site-specific water management, such as earlier drainage closure or supplemental irrigation. The combined time series of groundwater level, soil moisture, and subsurface discharge, together with mapped peat/mineral stratigraphy, can be used for coupled hydrology–biogeochemistry models and the estimation of scenario-based N and P leaching and GHG emissions under alternative drainage controls and climates. A better understanding of these hydrological dynamics helps to improve drainage management strategies to mitigate nutrient leaching and GHG emissions, ultimately enhancing the sustainability of peatland agriculture under changing climate conditions.

CRediT authorship contribution statement

Tung Pham: Writing – review & editing, Writing – original draft, Visualization, Methodology, Formal analysis, Data curation. **Hannu Marttila:** Writing – review & editing, Supervision, Project administration, Investigation, Funding acquisition. **Miika Läpikivi:** Writing – review & editing, Investigation, Data curation. **Timo Lötjönen:** Writing – review & editing, Methodology, Investigation, Data curation. **Hermanni Aaltonen:** Writing – review & editing, Investigation. **Henriikka Vekuri:** Writing – review & editing, Methodology, Data curation. **Bjørn Kløve:** Supervision, Project administration, Funding acquisition. **Maarit Liimatainen:** Writing – review & editing, Supervision, Project administration, Funding acquisition.

Declaration of competing interest

The authors declare that they have no known competing financial interests or personal relationships that could have appeared to influence the work reported in this paper.

Acknowledgement

This work was supported by the Suoviljelysyhdistys Foundation; the RATKU and TURVA projects, funded by the European Regional Development Fund (ERDF) through the Centre for Economic Development, Transport and the Environment of Northern Ostrobothnia; the Kone Foundation; Maa- ja vesitekniikan tuki ry; the TurvePäästö and ViljaPäästö projects, funded by the European Agricultural Fund for Rural Development through the Centre for Economic Development, Transport and the Environment of Northern Ostrobothnia; Oulun läänin talousseuran maataloussäätiö; WaterPeat—Water management for sustainable use and protection of peatlands funded by the WaterWorks 2017 ERA-NET Cofund; PeatWise—Wise use of drained peatlands in a bio-based economy: development of improved assessment practices and sustainable techniques for mitigation of greenhouse gases, funded by the JPI FACCE ERA-GAS ERA-Net Cofund; the VÄPÄ project, funded by the Ministry of Agriculture and Forestry from Catch the Carbon program and the TurPo project, funded by the Centre for Economic Development, Transport and the Environment of Northern Ostrobothnia and Ministry of the Environment. Erkki Joki-Tokola is appreciated for the development work of the NorPeat facility and Ruukki research infrastructure. We acknowledge the staff from Luke Ruukki experimental station for maintaining the research site and conducting measurements related to this study.

Appendix A. Supplementary data

Supplementary data to this article can be found online at https://doi.org/10.1016/j.jhydrol.2025.134461.

Data availability

Data will be made available on request.

References

AnaEE, 2025. European network for Analysis and Experimentation on Ecosystems Finland. AnaEE Finland. https://anaee.fi/facility/norpeat/.

Berglund, Ö., Berglund, K., 2011. Influence of water table level and soil properties on emissions of greenhouse gases from cultivated peat soil. Soil Biol. Biochem. 43 (5). https://doi.org/10.1016/j.soilbio.2011.01.002.

Bonn, A., Allott, T., Evans, M., Joosten, H., Stoneman, R., 2016. Peatland restoration and ecosystem services: Nature-based solutions for societal goals. In: Bonn, A., Allott, T., Evans, M., Joosten, H., Stoneman, R. (Eds.), Peatland Restoration and Ecosystem Services, 1st ed.,. Cambridge University Press, pp. 402–417. https://doi.org/10.1017/CBO9781139177788.021.

Chen, T., Guestrin, C., 2016. XGBoost: A scalable tree boosting system. In: Proceedings of the 22nd ACM SIGKDD International Conference on Knowledge Discovery and Data Mining, pp. 785–794. https://doi.org/10.1145/2939672.2939785.

Cobb, A.R., Harvey, C.F., 2019. Scalar simulation and parameterization of water table dynamics in tropical peatlands. Water Resour. Res. 55 (11). https://doi.org/10.1029/2019WR025411.

Cobb, A.R., Hoyt, A.M., Gandois, L., Eri, J., Dommain, R., Salim, K.A., Kai, F.M., Su'ut, N. S.H., Harvey, C.F., 2017. How temporal patterns in rainfall determine the geomorphology and carbon fluxes of tropical peatlands. Proc. Nat. Acad. Sci. USA 114 (26). https://doi.org/10.1073/pnas.1701090114.

Drösler, M., Freibauer, A., Christensen, T.R., Friborg, T., 2008. Observations and status of peatland greenhouse gas emissions in Europe. In: Dolman, A.J., Valentini, R., Freibauer, A. (Eds.), The Continental-Scale Greenhouse Gas Balance of Europe. Springer, pp. 243–261. https://doi.org/10.1007/978-0-387-76570-9_12.

European Commission. Joint Research Centre. Institute for Environment and Sustainability, 2008. Soils of the European Union. Publications Office. https://data.europa.eu/doi/10.2788/87029.

Evans, C.D., Peacock, M., Baird, A.J., Artz, R.R.E., Burden, A., Callaghan, N., Chapman, P.J., Cooper, H.M., Coyle, M., Craig, E., Cumming, A., Dixon, S., Gauci, V., Grayson, R.P., Helfter, C., Heppell, C.M., Holden, J., Jones, D.L., Kaduk, J., Morrison, R., 2021. Overriding water table control on managed peatland greenhouse gas emissions. Nature 593 (7860). https://doi.org/10.1038/s41586-021-03523-1.

van Genuchten, M.T., 1980. A closed-form equation for predicting the hydraulic conductivity of unsaturated soils. Soil Sci. Soc. Am. J. 44 (5), 892–898. https://doi.org/10.2136/sssaj1980.03615995004400050002x.

Gerin, S., Vekuri, H., Liimatainen, M., Tuovinen, J.P., Kekkonen, J., Kulmala, L., Laurila, T., Linkosalmi, M., Liski, J., Joki-Tokola, E., Lohila, A., 2023. Two contrasting years of continuous N2O and CO2 fluxes on a shallow-peated drained

agricultural boreal peatland. Agric. For. Meteorol. 341. https://doi.org/10.1016/j.agrformet.2023.109630.
Gharedaghloo, B., Price, J.S., Rezanezhad, F., Quinton, W.L., 2018. Evaluating the hydraulic and transport properties of peat soil using pore network modeling and X-ray micro computed tomography. J. Hydrol. 561, 494–508. https://doi.org/10.1016/j.jhydrol.2018.04.007.
Grønlund, A., Hauge, A., Hovde, A., Rasse, D.P., 2008. Carbon loss estimates from cultivated peat soils in Norway: a comparison of three methods. Nutr. Cycl. Agroecosyst. 81 (2), 157–167. https://doi.org/10.1007/s10705-008-9171-5.
Holden, J., Evans, M.G., Burt, T.P., Horton, M., 2006. Impact of land drainage on peatland hydrology. J. Environ. Qual. 35 (5), 1764–1778. https://doi.org/10.2134/jeq2005.0477.
Jury, W.A., Horton, R., 2004. Soil physics, 6th ed. John Wiley & Sons.
Kajasilta, H., Gerin, S., Niiranen, M., Läpikivi, M., Liimatainen, M., Kraus, D., Vekuri, H., Korkiakoski, M., Kulmala, L., Liski, J., Vira, J., 2025. The effects of peat thickness and water table depth on CO_2 and N_2O emissions from agricultural peatlands – a process-based modelling approach. Egusphere. https://doi.org/10.5194/egusphere-2025-4219 (Discussion Preprint).
Koch, J., Elsgaard, L., Greve, M.H., Gyldenkærne, S., Hermansen, C., Levin, G., Wu, S., Stisen, S., 2023. Water-table-driven greenhouse gas emission estimates guide peatland restoration at national scale. Biogeosciences 20, 2387–2403. https://doi.org/10.5194/bg-20-2387-2023.
Kormann, R., Meixner, F.X., 2001. An analytical footprint model for non-neutral stratification. Bound.-Lay. Meteorol. 99 (2), 207–224. https://doi.org/10.1023/A:1018991015119.
Laurila, T., Tuovinen, J., Lohila, A., Hatakka, J., Aurela, M., Thum, T., Pihlatie, M., Rinne, J., Vesala, T., 2005. Measuring methane emissions from a landfill using a cost-effective micrometeorological method. Geophys. Res. Lett. 32 (19), 2005GL023462. https://doi.org/10.1029/2005GL023462.
Limpens, J., Berendse, F., Blodau, C., Canadell, J.G., Freeman, C., Holden, J., Roulet, N., Rydin, H., Schaepman-Strub, G., 2008. Peatlands and the carbon cycle: from local processes to global implications—a synthesis. Biogeosciences 5 (5). https://doi.org/10.5194/bg-5-1475-2008.
Tähtikarhu, M., Räsänen, T.A., Hyväluoma, J., Piayda, A., Myllys, M., 2025. Analysing hydrological impacts of controlled drainage, peat thickness and groundwater fluxes in cultivated peat soils. Acta Agric. Scand. Section B - Soil Plant Sci. https://doi.org/10.1080/09064710.2025.2454388.
Maljanen, M., Hytönen, J., Mäkiranta, P., Laine, J., Minkkinen, K., Martikainen, P.J., 2013. Atmospheric impact of abandoned boreal organic agricultural soils depends on hydrological conditions. Boreal Environ. Res. 18, 250–268.
Maljanen, M., Sigurdsson, B.D., Guðmundsson, J., Óskarsson, H., Huttunen, J.T., Martikainen, P.J., 2010. Greenhouse gas balances of managed peatlands in the Nordic countries – present knowledge and gaps. Biogeosciences 7 (9), 2711–2738. https://doi.org/10.5194/bg-7-2711-2010.
Mauder, M., Jung, M., Stoy, P., Nelson, J.A., Wanner, L., 2024. Energy balance closure at FLUXNET sites revisited. Agric. For. Meteorol. 358, 110235. https://doi.org/10.1016/j.agrformet.2024.110235.
McCarter, C.P.R., Rezanezhad, F., Quinton, W.L., Gharedaghloo, B., Lennartz, B., Price, J., Connon, R., Van Cappellen, P., 2020. Pore-scale controls on hydrological and geochemical processes in peat: Implications on interacting processes. Earth Sci. Rev. 207. https://doi.org/10.1016/j.earscirev.2020.103227.
Menberu, M.W., Marttila, H., Ronkanen, A.K., Haghighi, A.T., Kløve, B., 2021. Hydraulic and physical properties of managed and intact peatlands: application of the Van Genuchten-Mualem models to peat soils. Water Resour. Res. 57 (7). https://doi.org/10.1029/2020WR028624.
Minkkinen, K., Laine, J., 1998. Long-term effect of forest drainage on the peat carbon stores of pine mires in Finland. Can. J. For. Res. 28 (9), 1267–1275.
Morris, P.J., Davies, M.L., Baird, A.J., Balliston, N., Bourgault, M.-A., Clymo, R.S., Fewster, R.E., Furukawa, A.K., Holden, J., Kessel, E., Ketcheson, S.J., Kløve, B., Larocque, M., Marttila, H., Menberu, M.W., Moore, P.A., Price, J.S., Ronkanen, A.-K., Rosa, E., Wilkinson, S.L., 2022. Saturated hydraulic conductivity in northern peats inferred from other measurements. Water Resour. Res. 58 (11), e2022WR033181. https://doi.org/10.1029/2022WR033181.
Myllys, M., Sinkkonen, M., 2004. Viljeltyjen turve- ja multamaiden pinta-ala ja alueellinen jakauma Suomessa. Suo 55 (3–4), 53–60.
Pham, T., Yli-Halla, M., Marttila, H., Lötjönen, T., Liimatainen, M., Kekkonen, J., Läpikivi, M., Klöve, B., Joki-Tokola, E., 2023. Leaching of nitrogen, phosphorus and other solutes from a controlled drainage cultivated peatland in Ruukki Finland. Sci. Total Environ. 904, 166769. https://doi.org/10.1016/j.scitotenv.2023.166769.
Prijac, A., Gandois, L., Riahi, K., Tremblay, A., Garneau, M., 2023. Hydrological connectivity controls dissolved organic carbon exports in a peatland-dominated boreal catchment stream. Hydrol. Earth Syst. Sci. 27, 3935–3958. https://doi.org/10.5194/hess-27-3935-2023.
Rebmann, C., Kolle, O., Heinesch, B., Queck, R., Ibrom, A., Aubinet, M., 2012. Data acquisition and flux calculations. In: Aubinet, M., Vesala, T., Papale, D. (Eds.), Eddy covariance: A practical guide to measurement and data analysis. Springer, pp. 59–83. https://doi.org/10.1007/978-94-007-2351-1_3.
Reddy, K.R., DeLaune, R.D., Inglett, P.W., 2022. Biogeochemistry of wetlands: Science and applications, 2nd ed. CRC Press. 10.1201/9780429155833.
Regina, K., Sheehy, J., Myllys, M., 2015. Mitigating greenhouse gas fluxes from cultivated organic soils with raised water table. Mitig. Adapt. Strat. Glob. Chang. 20 (8). https://doi.org/10.1007/s11027-014-9559-2.
Rezanezhad, F., Price, J.S., Quinton, W.L., Lennartz, B., Milojevic, T., Van Cappellen, P., 2016. Structure of peat soils and implications for water storage, flow and solute transport: a review update for geochemists. Chem. Geol. 429, 75–84. https://doi.org/10.1016/j.chemgeo.2016.03.010.
Ritzema, H.P. (Ed.), 2006. Drainage Principles and Applications (3rd ed.). Wageningen: International Institute for Land Reclamation and Improvement (ILRI), Publication 16. (1125 pp).
Rosset, T., Binet, S., Rigal, F., Gandois, L., 2022. Peatland dissolved organic carbon export to surface waters: global significance and effects of anthropogenic disturbance. Geophys. Res. Lett. 49 (5), e2021GL096616. https://doi.org/10.1029/2021GL096616.
Salla, A., Salo, H., Tähtikarhu, M., Marttila, H., Läpikivi, M., Liimatainen, M., Lötjönen, T., Koivusalo, H., 2024. Simulating controlled drainage and hydrological connections in a cultivated peatland field. Vadose Zone J. 23 (6), e20387. https://doi.org/10.1002/vzj2.20387.
van der Molen, W.H., Wesseling, J., 1991. A solution in closed form and a series solution to replace the tables for the thickness of the equivalent layer in Hooghoudt's drain spacing formula. Agric. Water Manag. 19 (1), 1–16. https://doi.org/10.1016/0378-3774(91)90058-Q.
Vekuri, H., Tuovinen, J.-P., Kulmala, L., Papale, D., Kolari, P., Aurela, M., Laurila, T., Liski, J., Lohila, A., 2023. A widely-used eddy covariance gap-filling method creates systematic bias in carbon balance estimates. Sci. Rep. 13 (1), 1720. https://doi.org/10.1038/s41598-023-28827-2.
Virtanen, K., 2003. Suomen turvevarat 2000. Geologian Tukimuskeskus.
Wallage, Z.E., Holden, J., 2011. Near-surface macropore flow and saturated hydraulic conductivity in drained and restored blanket peatlands. Soil Use Manag. 27 (2). https://doi.org/10.1111/j.1475-2743.2011.00336.x.
Wang, M., Bhowmik, A.K., Lennartz, B., 2020. Effect of anisotropy on solute transport in degraded fen peat. Hydrol. Process. 34 (21), 4106–4120. https://doi.org/10.1002/hyp.13717.
Xu, J., Morris, P.J., Liu, J., Holden, J., 2018. PEATMAP: refining estimates of global peatland distribution based on a meta-analysis. Catena 160. https://doi.org/10.1016/j.catena.2017.09.010.
Yli-Halla, M., Lötjönen, T., Kekkonen, J., Virtanen, S., Marttila, H., Liimatainen, M., Saari, M., Mikkola, J., Suomela, R., Joki-Tokola, E., 2022. Thickness of peat influences the leaching of substances and greenhouse gas emissions from a cultivated organic soil. Sci. Total Environ. 806, 150499. https://doi.org/10.1016/J.SCITOTENV.2021.150499.
Zak, D., Wagner, C., Payer, B., Augustin, J., Gelbrecht, J., 2010. Phosphorus mobilization in rewetted fens: the effect of altered peat properties and implications for their restoration. Ecol. Appl. 20 (5), 1336–1349. https://doi.org/10.1890/08-2053.1.